Photoacoustic and Fluorescence Image-Guided Surgery Using a Multifunctional Targeted Nanoprobe

Lei Xi, *University of Florida*
Guangyin Zhou, *University of Florida*
Ning Gao, *Emory University*
Lily Yang, *Emory University*
David A. Gonzalo, *University of Florida*
Steven J. Hughes, *University of Florida*
Huabei Jiang, *University of Florida*

Journal Title: Annals of Surgical Oncology
Volume: Volume 21, Number 5
Publisher: Springer Verlag (Germany) | 2014-05-01, Pages 1602-1609
Type of Work: Article | Post-print: After Peer Review
Publisher DOI: 10.1245/s10434-014-3541-9
Permanent URL: https://pid.emory.edu/ark:/25593/rnfhg

Final published version: http://dx.doi.org/10.1245/s10434-014-3541-9

HHS Public Access

Author manuscript

Ann Surg Oncol. Author manuscript; available in PMC 2016 June 15.

Published in final edited form as:

Ann Surg Oncol. 2014 May ; 21(5): 1602–1609. doi:10.1245/s10434-014-3541-9.

Photoacoustic and Fluorescence Image-Guided Surgery Using a Multifunctional Targeted Nanoprobe

Lei Xi, PhD[1], **Guangyin Zhou, PhD**[2], **Ning Gao, PhD**[3], **Lily Yang, MD, PhD**[3], **David A. Gonzalo, MD**[4], **Steven J. Hughes, MD**[2], and **Huabei Jiang, PhD**[1]

Huabei Jiang: hjiang@bme.ufl.edu

[1]Department of Biomedical Engineering, University of Florida, Gainesville, FL

[2]Department of Surgery, University of Florida, Gainesville, FL

[3]Department of Surgery, Emory University School of Medicine, Atlanta, GA

[4]Department of Pathology, University of Florida, Gainesville, FL

Abstract

Purpose—A complete surgical excision with negative tumor margins is the single most important factor in the prediction of long-term survival for most cancer patients with solid tumors. We hypothesized that image-guided surgery using nanoparticle-enhanced photoacoustic and fluorescence imaging could significantly reduce the rate of local recurrence.

Methods—A murine model of invasive mammary carcinoma was utilized. Three experimental groups were included: (1) control; (2) tumor-bearing mice injected with non-targeted nanoprobe; and (3) tumor-bearing mice injected with targeted nanoprobe. The surgeon removed the primary tumor following the guidance of photoacoustic imaging (PAI), then inspected the surgical wound and removed the suspicious tissue using intraoperative near-infrared (NIR) fluorescence imaging. The mice were followed with bioluminescence imaging weekly to quantify local recurrence.

Results—Nanoprobe-enhanced photoacoustic contrast enabled PAI to map the volumetric tumor margins up to a depth of 31 mm. The targeted nanoparticles provided significantly greater enhancement than non-targeted nano-particles. Seven mice in the group injected with the targeted nanoprobes underwent additional resections based upon NIR fluorescence imaging. Pathological analysis confirmed residual cancer cells in the re-resected specimens in 5/7 mice. Image-guided resection resulted in a significant reduction in local recurrence; 8.7 and 33.3 % of the mice in the targeted and control groups suffered recurrence, respectively.

Conclusions—These results suggest that photoacoustic and NIR intraoperative imaging can effectively assist a surgeon to locate primary tumors and to identify residual disease in real-time. This technology has promise to overcome current clinical challenges that result in the need for second surgical procedures.

Surgery remains the most effective treatment for the majority of cancer patients in the early stage of solid cancers.[1] Incomplete tumor excision is strongly associated with local

DISCLOSURES No potential conflicts of interest were disclosed.

recurrence and impacts survival rates.[2–5] Currently, operative procedures are dependent upon the experience and skill of the surgeon.[6] The development of image-guided surgery represents an opportunity to address two major surgical problems: (1) non-invasively locate a tumor that is invisible to the naked eye; and (2) facilitate complete removal of the tumor through detection of residual disease.

So far, a number of imaging-guided tools have been forwarded to achieve these goals, including mechanical, electromagnetic, and optical navigation systems.[7–9] Of these options, optical imaging technologies appear to be ideal since they can be miniaturized and are inexpensive, rapid, and sensitive. A number of optical navigational systems using elastic scattering spectroscopy (ESS), Raman spectroscopy, optical coherence tomography (OCT) or diffuse reflectance spectroscopy (DRS) have been investigated for their potential use in image-guided surgery.[10–13] However, all of these methods cannot provide sufficient depth information for tumor localization since their maximal sensing depth is limited, from 300 μm to 2 mm. Diffuse optical tomography (DOT) and fluorescence molecular tomography (FMT) can overcome the limitations associated with these surface-weighted imaging methods.[14,15] However, both have a limited spatial resolution (~1–2 mm) which is probably insufficient for intraoperative imaging.

Laser-induced photoacoustic imaging (PAI) is an emerging image modality that is capable of combining rich optical contrast with high acoustic spatial resolution (30 μm–1 mm, adjustable with ultrasound frequency).[16,17] Our previous study of a microelectromechanical systems (MEMS)-based, intraoperative, photoacoustic imaging probe demonstrated the clinical potential of PAI to non-invasively map the volumetric margins of breast tumors.[18,19] The challenge remaining for PAI is its capability to map tumors located several centimeters beneath the tissue surface. To overcome this limitation, photoacoustic contrast agents have been investigated and widely reported to improve the penetration ability of PAI. A variety of photoacoustic contrast agents have now been developed for this purpose, including magnetic iron oxide nanoparticles (IONPs), carbon nanotubes, gold nanocages, gold nanorods, and gold nanoshells for imaging breast tumors, brain tumors, angiogenesis, melanomas, lymph nodes, and the cerebral cortex.[20–24] Of all these contrast agents, IONPs appear the most promising with modest light absorption in near-infrared (NIR) wavelengths, small size (10 nm), long retention time in tissues, and multifunctionality.[25] In our previous study, we reported the use of NIR dye-labeled amino-terminal fragments (ATFs) of urokinase plasminogen activator (uPA) conjugated magnetic IONPs (NIR-830–ATF–IONPs) that target the uPA receptor (uPAR) to enhance the photoacoustic contrast of breast tumors in mice. Systemic delivery of the nanoprobe into the mice bearing mammary tumors led to a significant improvement in the photoacoustic signals and enabled PAI to image tumors located as deep as 31 mm beneath the tissue surface.[26] These results showed clinical potential of uPAR-targeted PAI to locate the primary tumors. However, the relatively low temporal resolution (minutes) and requirement of matching medium for the transmission of photoacoustic signals make PAI infeasible for imaging the surgical bed to detect the residual disease.

Currently, real-time, non-contact NIR fluorescence imaging combined with targeted/non-targeted NIR dye-labeled probes is a promising approach to detect either a superficial

primary tumor or residual disease within an operative resection bed. To date, many groups have successfully combined NIR fluorescence imaging with various NIR dyes to examine the residual neoplasia using animal models.[27–31] However, the imaging depth is limited (several millimeters) and resolution decreases dramatically as the imaging depth increases.

In the present study, we aimed to combine PAI with NIR fluorescence imaging to guide the resection in a murine mammary tumor model with mice bearing highly invasive 4T1 mammary tumor. Our goal was to demonstrate the feasibility of PAI to initially plan tumor resection, and then use NIR fluorescence imaging to guide further resection of potential residual disease when indicated. Importantly, we further aimed to determine if this approach had an impact on the development of local tumor recurrence.

METHODS

Cell Line, Animal Model and Preparation of Nanoprobes

Mouse mammary carcinoma 4T1 cells that stably express Luciferase, provided by Dr. Mark W. Dewhirst at Duke University, Durham, NC, USA, were cultured at 37 °C in a humidified incubator in Dulbecco's Modified Eagle's Medium supplemented with 10 % fetal bovine serum and antibiotics. Cells were harvested at 80 % confluence. 2×10^6 cells were implanted into the mammary fat pads of 6- to 8-week-old female BALB/c mice. Tumors were allowed to progress for 6–10 days to a size of 0.5–0.8 cm prior to randomization into one of the treatment groups. Animals were anesthetized using Isoflurane with precision vaporizer at 1–1.5 %, and were sacrificed using University of Florida Institutional Animal Care and Use Committee (IACUC)-approved techniques.

Recombinant ATFs were generated from pET101/D-TOPO expression vectors containing a mouse ATF of the receptor binding domain of uPA cDNA sequence and expressed in *Escherichia coli* BL21 (Invitrogen, Carlsbad, CA, USA). ATF peptides were purified from bacterial extracts with Ni^{2+} nitrilotri-acetic acid (NTA)-agarose columns (Qiagen, Valencia, CA, USA) and NIR dye (NIR-830) was synthesized using IR-783 (Sigma-Aldrich, St. Louis, MO, USA) using an established protocol.[25] ATF peptide or control bovine serum albumin proteins (BSA) were labeled with NIR-830 dye and then conjugated to amphiphilic polymer-coated, 10 nm magnetic IONPs (Oceannanotech, LLS, Springdale, AR, USA) via cross-linking of carboxyl groups of the amphiphilic polymer to the animo side groups of the peptides. Details can be found in our previous publications.[25,26]

Imaging Systems

A schematic of the PAI system is shown in Fig. 1a. A tunable Ti:Sapphire laser (LT-2211A, LOTIS TII) with 8–30 ns pulse duration and 10 Hz repetition rate was used. The laser beam was split and coupled into two optical fiber bundles. Induced photoacoustic waves were collected by a focused 3.5 MHz ultrasound transducer with 15 mm aperture and 35 mm focal length. The imaging probe consisting of transducer and optical fiber bundles was mounted on a two-dimensional (2D) moving stage that scanned two-dimensionally to form a three-dimensional (3D) image. The imaging area was 20 mm × 20 mm, with a 200 μm interval step. All in vivo experiments were performed with a light intensity of 8 mJ/cm^2 to

intentionally remain well below the American National Standards Institute safety limit (20 mJ/cm^2).

Figure 1b shows the schematic of the planar fluorescence imaging system. Two laser beams generated from two 785 nm CW lasers (M5-785-0080; Thorlabs, Newton, NJ) were coupled into optical fiber bundle I and optical fiber bundle II. An EMCCD equipped with a high-performance fluorescent band-pass filter (NT86-381; Edmund Optics, Barrington, NJ) was used to collect the fluorescence signals. All experiments were conducted using the same illumination pattern and camera exposure times.

Experimental Procedures

Mice were divided into three groups: Group 1 ($n = 12$) received an injection of 100 pmol NIR-830–ATF–IONPs; Group 2 ($n = 12$) received an injection of 100 pmol of NIR-830–BSA–IONPs; and Group 3 ($n = 15$) received no IONP injections. Tumors were resected following the guidance of photoacoustic images at 24 hours post-injection. Following the first excision, NIR fluorescence imaging was carried out to check the completeness of the surgery. If there were suspicious tissues, additional surgeries were performed to remove them.

Bioluminescence imaging (BMI) was carried out 14, 21, and 28 days post-surgery to track the local tumor recurrence using the IVIS Imaging System (Xenogen, PerkinElmer). Mice were sacrificed at 28 days or when the diameter of the recurrent tumor was greater than 1 cm.

Histological Analysis

After imaging, mice were sacrificed and tumors were excised and fixed with 10 % buffered formalin. Paraffin tissue sections were stained with Prussian blue (PB) or hematoxylin and eosin (H&E). All specimens were reviewed by the project pathologist who is an expert in clinical, surgical pathology. Images were acquired at 40× and 200× magnifications using a Zeiss Axioplan 2 upright microscope.

Statistical Analysis

For local recurrence between the targeted group and the control group, we used unpaired Student's t tests. Differences were considered significant when $p < 0.05$.

RESULTS

In this study, we first wanted to reproduce the findings reported in our previous work by demonstrating that the accumulation of NIR-830–ATF–IONPs in the tumor emitted much stronger optical signals compared with those of NIR-830–BSA–IONPs at 24 hours post-injection (Fig. 2a). The PB-stained tumor tissue sections obtained from mice injected with NIR-830–ATF–IONPs clearly showed the blue-stained clusters of IONPs. While no blue stained cluster of IONPs showed up in the section of tumor from the mice received an injection of NIR-830–BSA–IONPs.

To locate the tumor by PAI relative to surface landmarks, we marked the skin in the imaging region with four tiny markers of epoxy mixed with ink. A typical reconstructed 3D image of a tumor is shown in Fig. 2b. Following the maximum amplitude projection (MAP) of PAI and the cross-sections depicted in Fig. 2c, the surgeon used the profile of the tumor in the surgical area to excise it. Following the first surgery, the mouse was transferred to the platform of NIR fluorescence imaging and the operative bed was evaluated for residual disease. The guidelines for additional resection were developed by comparing the optical properties of tumor tissues in the surgical cavity with the normal tissues away from the surgical area (Fig. 3). First, we re-resected the tissue from the surgical area (*white dashed circle*, Fig. 3a). We then imaged it with the primary tumor and normal tissue from the area near the right leg (*yellow dashed circle*). Results in Fig. 3b suggest that the optical contrast of the tumor-free tissue from the surgical bed was lower than that of the primary tumor, but remained above levels that were observed in normal tissue from other areas (1.4:1). Histological section in Fig. 3c confirmed no tumor cells were included in the re-resected specimen. Thus, for subsequent operative procedures, we defined 1.4 as the trigger value of optical contrast for suspicious tissues. In reality, the optical contrast of all the re-resected suspicious tissues to the normal tissues was greater than 2. We observed two typical conditions where the mice needed further operations. Figure 4a represented the first one where we observed that the middle of the tumor bed emitted very strong optical signals, as strong as the primary tumor, suggesting suspicious tissue had invaded the underlying muscle. Subsequent analysis of these resected specimens did in fact demonstrate residual tumor cells invading skeletal muscle fibers.

Figure 4b demonstrates the other scenario we observed where optical properties of the tissues at the edge of the wound were suspicious after the first excision. We imaged the specimens resected from both surgeries and found that the specimen from the second surgery had the same optical contrast (3:1) compared with the primary tumor. The low-power magnification and high-power magnification histological sections in Fig. 4a, b confirmed the tumor cells within the re-resected specimens.

Following the surgical procedures, the mice were kept for 30 days and weekly BMI was conducted to identify local recurrence in the operative bed. Figure 4c shows the fully recovered mice. In both animal groups, we found mice with lymph node metastases and mice with local recurrences in the operative bed. As summarized in Table 1, 8.7 % of the mice in the targeted animal group and 33.3 % of the mice in control animal group developed local recurrence, and this difference was statistically significant ($p < 0.05$). We did not observe a local recurrence in any of the mice in the targeted animal group that underwent an additional resection; pathological analysis indicated that 71.4 % of the re-resected specimens contained residual neoplasm.

DISCUSSION

Unlike the conventional surgery procedures where the surgeon must depend on their eyes and hands to look for disease and make subjective decisions to excise tumors with disease-free margins in the operating room, the multi-functionality of NIR-830–ATF–IONP has the potential to serve as PAI contrast that offers the surgeon a 3D reconstruction of the tumor

located deep inside the tissue as well as NIR fluorescence imaging to detect residual diseases in the surgical cavity.

Besides high spatial resolution, deep penetration, and high sensitivity of dual imaging modality, this approach toward imaging intraoperatively had other advantages of nanoprobes that should be acknowledged. IONPs are a class of biodegradable and biocompatible nanoparticles with a low toxicity in humans, and have already been used in human patients for magnetic resonance imaging detection of liver cancer and lymph node metastasis.[32] The modified NIR-830 dye has significant advantages for imaging because of minimal interfering absorption and fluorescence from biologic samples, low-cost excitation laser diode, and enhanced penetration depth with emission wavelength at 700–850 nm.

In this study, we noticed that there were two different types of NIR-830–ATF–IONPs distributed in the mice. In some cases, the optical signal of the tumor was much stronger than that of the internal organs (liver, kidney). In other cases, the optical signal of the tumor was comparable with that of the internal organs (liver, kidney). It is possible that non-specific uptake of the IONPs by the reticuloendothelial system (RES) in the liver and kidney led to strong optical signals.[33–35] We also observed lymph node metastasis (30 %) in both targeted and control animal groups, an expected finding due to the aggressive malignant carcinoma cell line utilized. However, we did not detect any high-contrast optical signal in the lymph node in the experiments. There are two possible reasons for this: (1) the sensitivity of NIR fluorescence imaging was not high enough; and (2) a high optical signal of the liver overlapped with that of the lymph node.

We also recognized that these studies raised several concerns that may limit the full clinical potential of this technology. First, the present PAI system is bulky and slow and thus is not suitable for clinical applications, especially intraoperative imaging. However, this should not be a fundamental problem of PAI since the problem can be solved by using a commercial ultrasound array and/or a high frame rate of laser pulses with a high-speed scanning system.[36] Second, we need to confine the contrast criteria for suspicious tissues since two suspicious tissues met the criteria in the protocol, but we did not find any cancer cells in the histological sections. These results suggested that additional work will need to be performed to determine an optimum algorithm to drive re-resection. Third, our nanoparticle design needs to be modified to incorporate larger numbers of NIR-830-dye molecules (over 1,000 molecules per IONP) into the polymer coating of the IONPs, compared with currently used NIR-830 dye-labeled ATF–IONP with around 40 dye molecules per nanoparticle. Increased concentration of NIR dye in NIR-830–ATF–IONP may further enhance the sensitivity of both PAI and fluorescence imaging. Finally, it is possible to integrate a more sensitive intraoperative NIR imaging technique, such as Raman microscopy or handheld Raman probe, with a handheld planar fluorescence imaging to detect the residual disease with a higher sensitivity.[37]

CONCLUSIONS

In this report, we demonstrated the feasibility of combining PAI and NIR fluorescence imaging augmented by the systemic delivery of NIR-830–ATF–IONPs to guide the initial

resection and subsequent additional resections, if indicated, of a highly invasive breast carcinoma in a murine model. The results clearly showed that image-guided resection resulted in a significant reduction in the local recurrence rate. Besides breast cancer surgery, this approach also may have potential benefits for image-guided surgery in ovarian and pancreatic cancer patients.[33–35]

Acknowledgments

We thank Dr. Andrew Y. Wang at Ocean Nanotech, LLC, for providing magnetic IONPs, and Dr. Malgorzata Lipowska at Emory University for synthesis of NIR 830 dye. This research project was supported by the following National Institutes of Health (NIH) Grants: NIH R21CA 161384 (Huabei Jiang) and R01CA133722 (Lily Yang).

References

1. Aliperti LA, Predina JD, Vachani A, Singhal S. Local and systemic recurrence is the Achilles heel of cancer surgery. Ann Surg Oncol. 2011; 18:603–607. [PubMed: 21161729]
2. Taghian A, Mohiuddin M, Jagsi R, Goldberg S, Ceilley E, Powell S. Current perceptions regarding surgical margin status after breast-conserving therapy: results of a survey. Ann Surg. 2005; 241(4): 629–39. [PubMed: 15798465]
3. Assersohn L, Powles TJ, Ashley S, et al. Local relapse in primary breast cancer patients with unexcised positive surgical margins after lumpectomy, radiotherapy and chemoendocrine therapy. Ann Oncol. 1999; 10(12):1451–5. [PubMed: 10643535]
4. Balch GC, Mithani SK, Simpson JF, Kelley MC. Accuracy of intraoperative gross examination of surgical margin status in women undergoing partial mastectomy for breast malignancy. Am Surg. 2005; 71(1):22–7. [PubMed: 15757052]
5. Sigal-Zafrani B, Lewis JS, Clough KB, et al. Histological margin assessment for breast ductal carcinoma in situ: precision and implications. Mod Pathol. 2004; 17(1):81–8. [PubMed: 14657957]
6. Abraham SC, Fox K, Fraker D, Solin L, Reynolds C. Sampling of grossly benign breast reexcisions: a multidisciplinary approach to assessing adequacy. Am J Surg Pathol. 1999; 23:316–22. [PubMed: 10078923]
7. Marmulla R, Hilbert M, Niedert-Ellmann H. Intraoperative precision of mechanical, electromechanical, infrared and laser-guided navigation systems in computer-assisted surgery. Mund Kiefer Gesichtschir. 1998; 2:145–8.
8. Hassfeld S, Muhling J. Comparative examination of the accuracy of a mechanical and an optical system in CT and MRT based instrument navigation. Int J Oral Maxillofac Surg. 2000; 29(6):400–7. [PubMed: 11202318]
9. Wagner A, Schicho K, Birkfellner W, et al. Quantitative analysis of factors affecting intraoperative precision and stability of optoelectronic and electromagnetic tracking systems. Med Phys. 2002; 29(5):905–12. [PubMed: 12033587]
10. Bigio IJ, Bown SG, Briggs G, et al. Diagnosis of breast cancer using elastic-scattering spectroscopy: preliminary clinical results. J Biomed Opt. 2000; 5(2):221–8. [PubMed: 10938787]
11. Haka AS, Volynskaya Z, Gardecki JA, et al. In vivo margin assessment during partial mastectomy breast surgery using Raman spectroscopy. Cancer Res. 2006; 66(6):3317–22. [PubMed: 16540686]
12. Kennedy S, Geradts J, Bydlon T, et al. Optical breast cancer margin assessment: an observational study of the effects of tissue heterogeneity on optical contrast. Breast Cancer Res. 2010; 12(6):R91. [PubMed: 21054873]
13. Nguyen FT, Zysk AM, Chaney EJ, et al. Intraoperative evaluation of breast tumor margins with optical coherence tomography. Cancer Res. 2009; 69(22):8790–6. [PubMed: 19910294]
14. Yang H, Xi L, Samuelson S, Xie H, Yang L, Jiang H. Handheld miniature probe integrating diffuse optical tomography with photoacoustic imaging through a MEMS scanning mirror. Biomed Opt Express. 2013; 4:427–32. [PubMed: 23504287]

15. He B, Xi L, Samuelson SR, Xie H, Yang L, Jiang H. Micro-electromechanical systems scanning-mirror-based handheld probe for fluorescence molecular tomography. Appl Opt. 2012; 51:4678–83. [PubMed: 22781242]
16. Wang LV. Multiscale photoacoustic microscopy and computed tomography. Nat Photonics. 2009; 3(9):503–9. [PubMed: 20161535]
17. Beard P. Biomedical photoacoustic imaging. Interface Focus. 2011; 1:602–31. [PubMed: 22866233]
18. Xi L, Sun J, Zhu Y, Wu L, Xie H, Jiang H. Photoacoustic imaging based on MEMS mirror scanning. Biomed Opt Express. 2010; 1:1278–83. [PubMed: 21258548]
19. Xi L, Grobmyer SR, Wu L, et al. Evaluation of breast tumor margins in vivo with intraoperative photoacoustic imaging. Opt Express. 2012; 20:8726–31. [PubMed: 22513583]
20. Pan D, Pramanik M, Senpan A, et al. Molecular photoacoustic imaging of angiogenesis with integrin targeted gold nanobeacons. FASEB J. 2011; 25(3):875–82. [PubMed: 21097518]
21. Kim C, Cho EC, Chen J, et al. In vivo molecular photoacoustic tomography of melanomas targeted by bioconjugated gold nanocages. ACS Nano. 2010; 4:4559–64. [PubMed: 20731439]
22. Pan D, Pramanik M, Senpan A, Ghosh S, Wickline SA, Wang LV, et al. Near infrared photoacoustic detection of sentinel lymph nodes with gold nanobeacons. Biomaterials. 2010; 31:4088–93. [PubMed: 20172607]
23. Kim C, Song KH, Gao F, Wang LV. Sentinel lymph nodes and lymphatic vessels: noninvasive dual-modality in vivo mapping by using indocyanine green in rats-volumetric spectroscopic photoacoustic imaging and planar fluorescence imaging. Radiology. 2010; 255:442–50. [PubMed: 20413757]
24. Yang XM, Skrabalak SE, Li Z, Xia Y, Wang LV. Photoacoustic tomography of a rat cerebral cortex in vivo with au nanocages as an optical contrast agent. Nano Lett. 2007; 7(12):3798–802. [PubMed: 18020475]
25. Yang L, Peng XH, Wang A, et al. Receptor-targeted nanoparticles for in vivo imaging of breast cancer. Clin Cancer Res. 2009; 15:4722–32. [PubMed: 19584158]
26. Xi L, Grobmyer SR, Zhou G, Qian W, Yang L, Jiang H. Molecular photoacoustic tomography of breast cancer using receptor targeted magnetic iron oxide nanoparticles as contrast agents. J Biophotonics.
27. De Grand AM, Frangioni JV. An operational near-infrared fluores-cence imaging system prototype for large animal surgery. Technol Cancer Res Treat. 2003; 2:553–62. [PubMed: 14640766]
28. Tanaka E, Choi HS, Fujii H, Bawerndi MG, Frangion JV. Image-guided oncologic surgery using invisible light: completed pre-clinical development for sentinel lymph node mapping. Ann Surg Oncol. 2006; 13:1671–81. [PubMed: 17009138]
29. Troyan SL, Kianzad V, Gibbs-Strauss SL, et al. The FLARE^{TM} intraoperative near-infrared fluorescence imaging system: a first-in-human clinical trial in breast cancer sentinel lymph node mapping. Ann Surg Oncol. 2009; 16:2943–52. [PubMed: 19582506]
30. Gioux S, Kianzad V, Ciocan R, Gupta S, Oketokoun R, Frangion JV. High-power, computer-controlled, light-emitting diode-based light sources for fluorescence imaging and image-guided surgery. Mol Imaging. 2009; 8(3):156–65. [PubMed: 19723473]
31. Van Dam GM, Themelis G, Crane LM, et al. Intraoperative tumor-specific fluorescence imaging in ovarian cancer by folate receptor-α targeting: first in-human results. Nat Med. 2011; 17:1315–9. [PubMed: 21926976]
32. Harisinghani MG, Barentsz J, Hahn PF, et al. Noninvasive detection of clinically occult lymph-node metastases in prostate cancer. N Engl J Med. 2003; 348(25):2491–9. [PubMed: 12815134]
33. Satpathy M, Wang L, Zielinski R, et al. Active targeting using HER-2-affibody-conjugated nanoparticles enabled sensitive and specific imaging of orthotopic HER-2 positive ovarian tumors. Small. 2013; 10(3):544–55. DOI: 10.1002/Smll01593 [PubMed: 24038985]
34. Xi L, Minati S, Zhao Q, Qian W, Yang L, Jiang H. HER-2/Neu targeted delivery of a nanoprobe enabled dual photoacoustic and fluorescence tomography of ovarian cancer. Nanomedicine. 2013; doi: 10.1016/J.Nano.11.004

35. Yang L, Mao H, Cao Z, et al. Molecular imaging of pancreatic cancer in an animal tumor model using targeted multifunctional nanoparticles. Gastroenterology. 2009; 136(5):1514–25. [PubMed: 19208341]

36. Erpelding TN, Kim C, Pramanik M, et al. Sentinel lymph nodes in the rat: noninvasive photoacoustic and US imaging with a clinical US system. Radiology. 2010; 256(1):102–10. [PubMed: 20574088]

37. Mohs AM, Mancini MC, Singhal S, Provenzale JM, Leyland-Jones B, Wang MD, et al. Hand-held spectroscopic device for in vivo and intraoperative tumor detection: contrast enhancement, detection sensitivity, and tissue penetration. Anal Chem. 2010; 82(21):9058–65. [PubMed: 20925393]

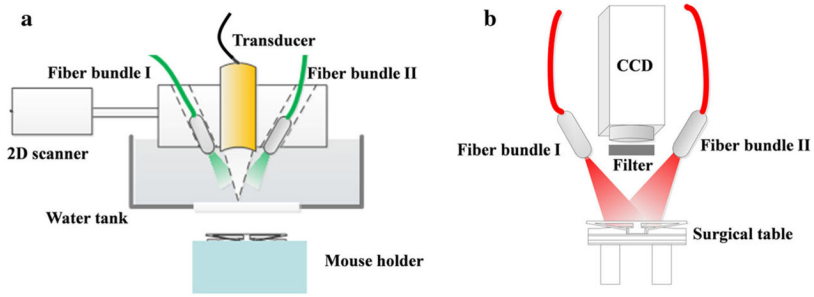

FIG. 1.

Schematic of the **a** PAI system and **b** NIR fluorescence imaging system. *PAI* photoacoustic imaging, *NIR* near-infrared

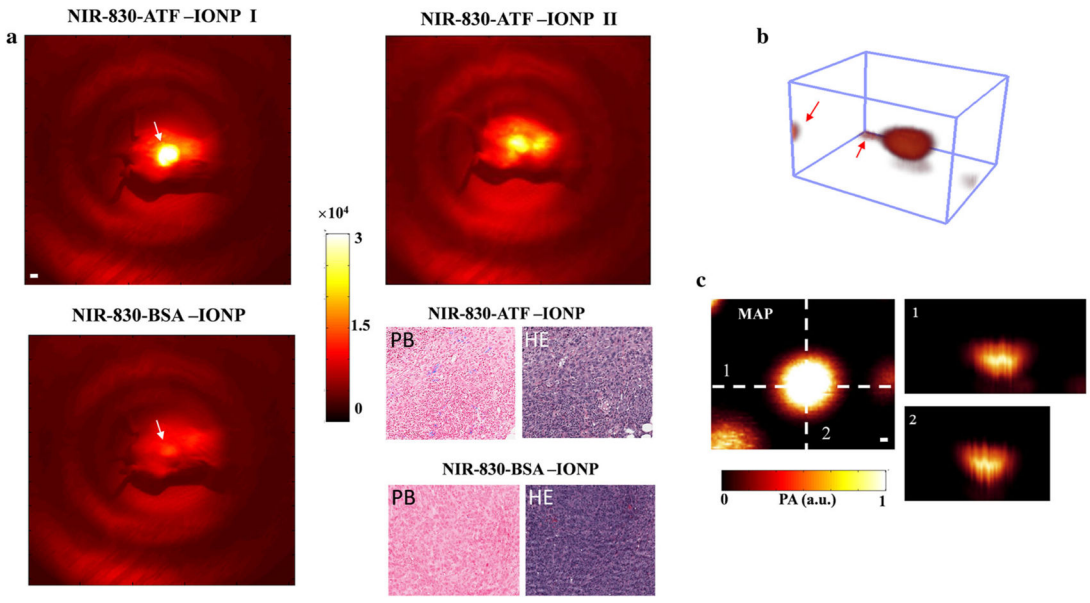

FIG. 2.

Validation of targeting ability and contrast enhancement for PAI of NIR-830–ATF–IONPs. **a** NIR fluorescence imaging of mice that received an injection of NIR-830–ATF–IONPs or NIR-830–BSA–IONPs. All tumors from the targeted animal group had strong optical signals and some showed strong signals from the internal organs (kidney and liver), possibly due to the non-specific uptake of the IONP by the RES in the liver and elimination of degraded NIR-830-dye-conjugates in the kidney. PB-stained tumor tissue sections from the mice injected with NIR-830–ATF–IONPs showed a cluster of blue-stained IONPs, while no blue-stained IONPs were found in the mice injected with NIR-830–BSA–IONPs. **b** A typical three-dimensional photoacoustic image with two tiny markers in the corners. Markers indicated by the *red arrows* were used to assistant surgeons in locating the tumors in the imaging area. **c** MAP and cross-sections of photoacoustic image shown in **b**. The MAP images were used to depict the surgical profile in the imaging area, and cross-sections provided depth information and axial dimension of tumors. *NIR* near-infrared, *IONPs* iron oxide nanoparticles, *RES* reticuloendothelial system, *MAP* maximum amplitude projection

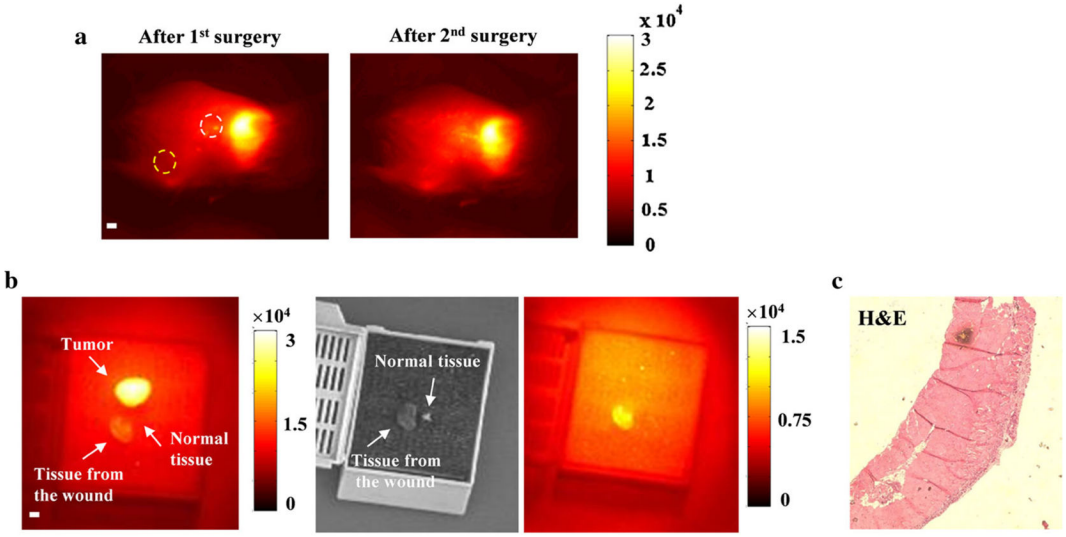

FIG. 3.

Establishment of a protocol for identifying suspicious tissues with residual diseases. **a** Following the PAI-guided surgery, two pieces of tissues from the area in (*white dashed circles*) and away from (*yellow dashed circle*) the surgical bed were resected and imaged with the primary tumor. **b** Both the primary tumor and the tumor-free specimen resected from the wound (*white circle*) emitted stronger optical signals compared with the specimen resected from the area away from the surgical wound (*yellow circle*). The optical intensity difference between two re-resected specimens was caused by the inhomogeneous illumination pattern. In the following experiments, 1.4 was set to be the cutoff value of contrast for suspicious tissues. **c** Histological section of the tumor-free specimen resected from the wound. *Scale bar* 1 mm. *PAI* photoacoustic imaging, *H&E* hematoxylin and eosin

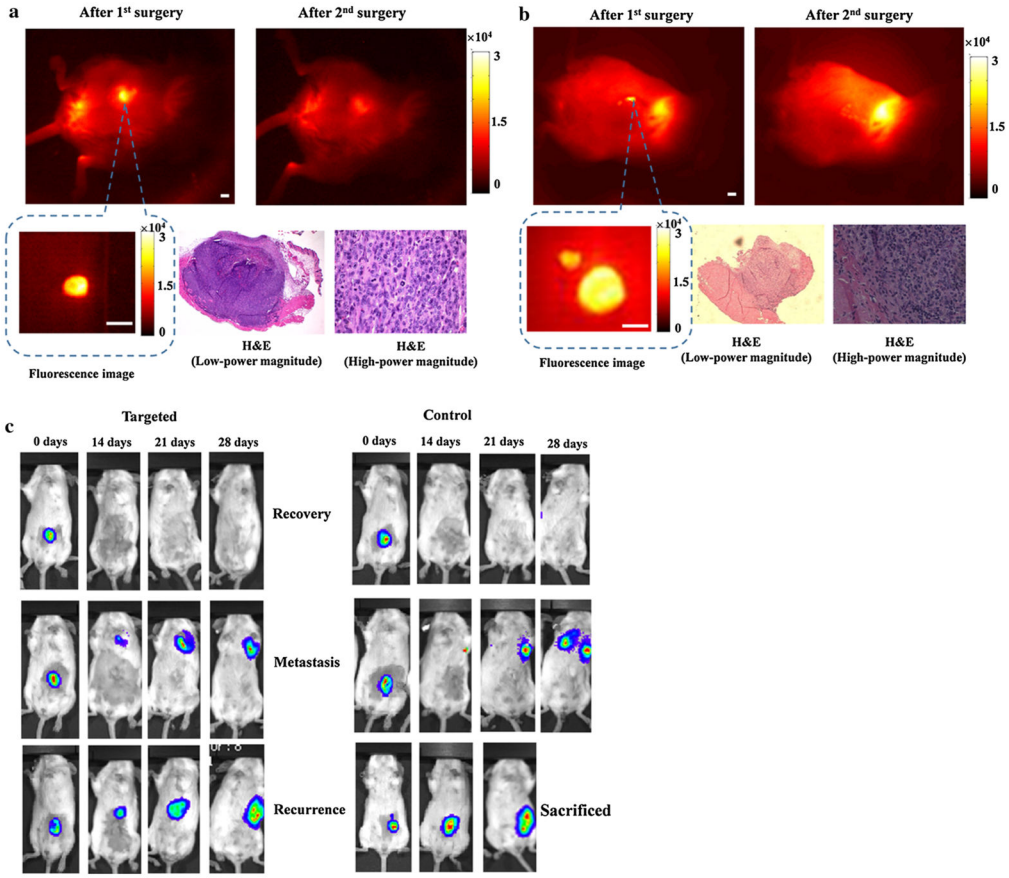

FIG. 4.

Fluorescent detection of residual disease in the surgical bed after incomplete resection and BMI to track local recurrence in the surgical bed. **a** The mouse was imaged after surgically removing the primary tumor guided by PAI. The residual disease could not be visualized by the surgeon; however, it was clearly detected by the NIR fluorescence imaging system. After additional surgery, no residual disease was detected. The contrast of the suspicious tissue was approximately 3:1 compared with the background normal tissue. The high-power magnification and low-power magnification histological sections confirmed the tumor cells in this specimen. *Scale bar* 2 mm. **b** The invisible small residual disease was fluorescently detected by the intraoperative planar fluorescence imaging system. Although the size of the suspicious tissue was much smaller than the primary tumor in this figure, the contrast was almost the same (3:1). H&E staining confirmed the presence of residual cancer cells in the suspicious tissues. Higher magnification microscopic image of the tumor tissue section showed the residual nodule interface. *Scale bar* 2 mm. **c** BMI on the 14th, 21st, and 28th day post-operation. Overall, 8.7 and 33.3 % of the mice in the targeted and control animal groups, respectively, had local recurrence, and approximately 30 % of the mice in both groups had lymph node metastasis. In the control group, most recurrent tumors grew larger than 1 cm within 3 weeks post-operation. *BMI* bioluminescence imaging, *PAI* photoacoustic imaging, *NIR* near-infrared, *H&E* hematoxylin and eosin

TABLE 1

Summary of tumor recurrence in mice in both groups

Group	Number	Tumor bed	Recurrence (%)
Targeted[a]	12	1	8.7
Re-resected[b]	7	0	0
Control[a]	15	5	33.3

[a]The difference (p <0.05) between the targeted group and the control group is significant

[b]The pathological results confirmed residual cancer cells in five of seven re-resected specimens